Journal: Nature Physics

Supplementary Information for:

"Fluctuation theorem experiment for entropy production in a strongly coupled plasma"

C.-S. Wong, J. Goree, Z. Haralson, B. Liu

Table of Contents of Supplementary Information

A. Details of the experimental method and parameters

Our plasma was made by evacuating air from the metal vacuum chamber of Ref. [18], filling it with argon to a pressure of 6.0 mTorr, and applying a peak-to-peak voltage of 100 V at 13.56 MHz between a horizontal electrode and the chamber wall, which acted as the other electrode. We then added ≈10^4 melamine-formaldehyde microspheres of 8.69 μm diameter. Each microsphere accumulated a charge Q = -15,000*e* on average, where *e* is the elementary charge. The microspheres were electrically levitated due to a dc bias of -61 V on the horizontal electrode. The charged microspheres maintained a spacing that corresponded to a Wigner-Seitz radius a = 0.33 mm, where $a = (n\pi)^{-1/2}$ and n is the areal number density. A typical microsphere moved with a velocity of only millimeters per second, due to its large mass, which was 7.82×10^{12} times greater than an argon atom.

The collection of microspheres is an open system that interacts with the other charged components of the dusty plasma (electrons and positive ions). Three important effects of the electrons and ions on the microspheres are

(1) the charging of microspheres (which depends on the floating potential of the microspheres)
(2) the screening of the interaction between microspheres
(3) the levitation and confinement of microspheres.

The first two effects determine the interaction potentials between microspheres, and in turn, the strength of collisions between microspheres. For our experiment, both the charge and screening are essentially steady, so that the strength of collisions between microspheres does not change noticeably during the experiment. Further details on charging and screening are given in Section C1 of the Supplementary Information.

To control the kinetic temperature of the microspheres and to sustain a steady shear flow, we used two pairs of laser beams.

- One pair of moving beams provided heating[24] so that the kinetic temperature was raised to a level of T = 99,300 K = $1.47T_{melt}$. Here we use the melting point data of Ref. [32] to define T_{melt}. The heating beams provided heating using a 4-s sequence that repeated itself 4 times, each time flipping vertically or horizontally[24].

- The other pair provided shear; these beams were in the plane of the microspheres, where they imparted momentum through the radiation pressure force. The shear laser beams were directed in the +x and -x directions. As shown in Fig. 1a, the shear laser beams were localized within a pair of stripes, each of which was 2 mm wide, and they were spaced 3 mm apart.

Tracking the microspheres yielded the experimental data. Images were recorded by a video camera, which viewed the microsphere layer from above at 60 frames/s. The 23.4 mm × 17.6 mm region that was viewed contained approximately 1100 microspheres. Particle tracking was done using optimized

image analysis methods[30,31,33] to yield time series data for the positions and velocities of individual microspheres.

Our experimental parameters were chosen so that the random thermal velocity of individual microspheres and the flow velocities were of the same order, 1 mm/s. Other experimental parameters include: nominal 2D dust plasma frequency[34] ω_{pd} = 74 s^{-1}; neutral gas friction force time constant[35,36] of 1.1 s^{-1}; shear rate (measured as the transverse gradient of the flow velocity between the shear beams) of γ = 0.58 s^{-1}; kinematic viscosity ν = 2.7 mm^2/s, obtained as in Ref. [26]; Reynolds number Re = 4; Coulomb coupling parameter[37] Γ = 114; and shielding parameter $\kappa = a/\lambda$ = 0.882.

B. Details of the calculation of the entropy production rate and the shear stress

1. Equations for computing the entropy production rate

Unlike many experiments for fluctuation theorems, ours centers on the measurement of the entropy production rate $\sigma(t)$. This measurement of $\sigma(t)$ is used as an input for Eq. (1), the fluctuation theorem of Evans, Cohen, and Morriss (ECM). In most other kinds of physic systems, it is not possible to measure $\sigma(t)$ within a small subsystem. However, for a dusty plasma experiment like ours with measurements of positions and velocities of individual microspheres in a shear flow, it is possible to obtain $\sigma(t)$ for a small number of particles. We computed the time average entropy production rate as

$$\sigma_\tau = \left\langle -\frac{P_{xy}(t)\gamma}{k_B T} \right\rangle_\tau , \tag{S1}$$

and the instantaneous entropy production rate as

$$\sigma(t) = -\frac{P_{xy}(t)\gamma}{k_B T} . \tag{S2}$$

The shear stress γ was computed as the transverse gradient of the flow velocity, the kinetic temperature *T* was obtained from the mean-square microsphere velocity after subtracting the local velocity, and the instantaneous shear stress $P_{xy}(t)$, which is specific to the *xy* plane, was calculated[26] according to

$$P_{xy}(t) = \sum_{i=1}^{N} m\tilde{v}_{i,x}\tilde{v}_{i,y} + \frac{1}{2}\sum_{i=1}^{N}\sum_{j\neq i} r_{ij,y}F_{ij,x} . \tag{S3}$$

Here, $i = 1,\ldots,N$ labels the microspheres within a subsystem and the final sum is over all microspheres, which are labeled *j*. The inputs for the shear stress are the individual particle masses *m* and velocities relative to the background flow $\tilde{\mathbf{v}}$, interparticle distances **r**, and interparticle forces **F**.

Binary interparticle electric forces among the microspheres were computed as the gradient of a potential

$$F(r_{ij}) = -\nabla\phi(r_{ij}) . \tag{S4}$$

We modeled the pairwise potential of microspheres as a Debye-Hückel potential

$$\phi(r_{ij}) = \frac{Q^2}{4\pi\epsilon_0 r_{ij}} \exp\left(-r_{ij}/\lambda\right), \tag{S5}$$

which requires as inputs: microsphere charges Q, interparticle distances *r,* and a screening length λ. As we discuss below in Section B3, the only force that affects the shear stress and therefore the entropy production rate in the expressions above is the binary interparticle electric force.

The choice of the Debye-Hückel potential is justified experimental[38] as well as simulation[39] results from the literature. A key point is that all our microspheres remained in a single layer that was perpendicular to the ion flow. We recognize that the Debye-Hückel potential is not applicable in general in an ion flow due to wakefield effects, however, it has been shown to be applicable in the plane perpendicular to the ion flow, as in our experiment. The simulation of Lampe et al.[39] considered the full three-dimensional volume around an isolated microsphere, and the authors found that the Debye-Hückel potential accurately described the disturbance of the ion-electron background on a plane perpendicular to the ion flow. The experiment of Konopka et al.[38] demonstrated that the binary interaction of two microspheres was accurately described by the Debye-Hückel potential up to a distance of about 3 screening lengths; beyond that distance the experimental uncertainties in measuring the potential energy were too large. In any case, our calculation of the forces is dominated by microspheres within this distance of 3 screening lengths, so that it is irrelevant whether the potential is theoretically different for larger radii. The presence of any hypothetical attractive forces at much larger radii would have negligible effect on the viscous heating, which is dominated by collisions with nearest neighbors, which are all within about one screening length in our experiment.

2. Entropy production vs. entropy

Entropy production is a signature of a nonequilibrium process, and it is associated with irreversibility. Our microspheres, because they are undergoing a shear flow driven by external forces, comprise a nonequilibrium steady state. The entropy production rate that we calculate is associated with viscous heating due to this shear flow.

Entropy, on the other hand, is a description of an equilibrium. Our experiment is not an equilibrium, so we do not calculate an entropy.

3. Isolating the entropy production process for viscous heating

We are able to analyze just the entropy production associated with viscous heating, separately from other entropy production processes. This separateness owes to the separateness of the forces underlying the processes. For entropy production associated with viscous heating, the only force that enters into the standard expressions Eqs. (S2-S3) is the binary interparticle forces for a single component, the microspheres. These expressions do not depend on any other forces that are present, such as the radiation pressure force (for laser heating and driving the shear flow) or the frictional force experienced by one component of the dusty plasma moving relative to another. While these other forces can cause entropy production, they are associated with processes distinct from those described by Eqs. (S2-S3).

Our experiment's design allows a further simplification in the analysis for viscous heating: in Eqs. (S2-S3) we only need to compute the entropy production due to vector components in the x-y plane. In other words, in the experiment we need only to observe the positions, velocities, and forces in the x-y plane. This is so because the experiment was designed to have no shear in the y-z or x-z planes, so that the viscous heating for motion in those planes would be zero.

For these reasons, in the Letter we analyze just the entropy production rate associated with viscous heating among the microspheres, using only the x-y components of their positions, velocities, and forces. In the culmination of the Letter, we find that this well-defined entropy production rate obeys the ECM fluctuation theorem.

4. Selection of a subsystem of microspheres within the shear flow

In general, fluctuation theorems are of interest for small systems. In our experiment, we must choose a small subsystem within our larger experimental system. Unlike simulations of small systems that make use of periodic boundary conditions, our experimental data includes thousands of microspheres, too many for a fluctuation theorem. Here we present prescriptions for two methods that we devised to calculate $P_{xy}(t)$, one that we used in the Letter and another as well. We have verified using experimental data, that they yielded comparable results. Below we describe these two methods.

Both of our methods use Eq. (S3) to compute $P_{xy}(t)$. The key issue is how to select a subsystem of microspheres within the larger region viewed by our camera. The two methods differed according to what we held fixed, the number N of microspheres or the analyzed area. Both methods used a rectangular region, but the region is specified differently in the two methods. We used the fixed microspheres number approach for the results presented in the Letter. In both methods, we computed four separate time series of $P_{xy}(t)$ simultaneously for four spatial regions between the shear beams. The widths (y-component) and the centers of the rectangular regions were the same for both methods. The widths extended between the two shear laser beams, $9.0 < y < 11.5$ mm, while the centers of the rectangular regions were at x = 7.5, 10.3, 13.2, and 16.0 mm.

- In the *fixed microsphere number method*, for each video frame we slightly adjusted the area of the analyzed spatial region by "rubber-banding" the length.

  Rubber-banding method: increasing or decreasing the length (x-component) of the rectangular region so that the rectangle always included exactly N = 56 microspheres. This adjustment was done for each video frame while keeping two quantities fixed: the width (y-component) and center position of the rectangle. Sample time series of the instantaneous entropy production rate and shear stress computed using the rubber-banding method are presented in Supplementary Figure S1.

- In the *fixed area method*, we specified the rectangle's length, width, and center position, which all remained fixed. Consequently, the number of microspheres contained within it was not constant, but varied from frame to frame, as microspheres flowed in and out of the fixed rectangle. We chose the dimensions so that the time average of N was 55.6. The rms variation of N was $\pm$ 2.1 microspheres. The rectangle's aspect ratio was length / width = 3.0.

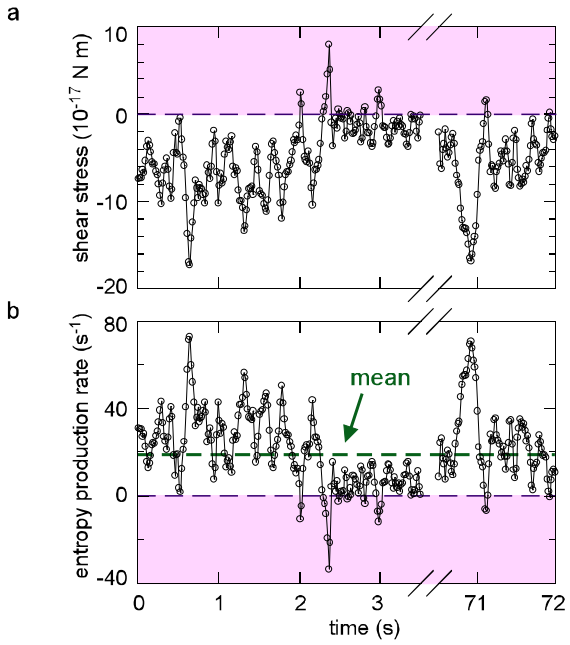

Supplementary Figure S1. **Shear stress and entropy production rate. a,** Sample time series of the shear stress $P_{xy}(t)$. Here, the shear stress was computed for $N = 56$ microspheres using the fixed number approach. The power spectrum obtained from a FFT of $P_{xy}(t)$ revealed no preferred frequency. **b,** Time series of the instantaneous entropy production rate computed from the shear stress as $\sigma(t) = -P_{xy}(t)\gamma / k_B T$. Since the shear rate γ and kinetic temperature T were constants, the entropy production rate is proportional to the shear stress. Note the negative fluctuations in the entropy production rate in the shaded region that correspond to the positive fluctuations of the shear stress. These are the events of interest for the fluctuation theorem

C. Experimental inputs for Eqs. (S1-S5) – how they were obtained, and how sensitive results are to these inputs

In this section, we discuss: the experimental inputs used in Eqs. (S1-S5) to compute the entropy production rate, the method we used to obtain these inputs, the uncertainties associated with each measurement, and the sensitivity of our result (that our strongly coupled plasma obeys the ECM fluctuation theorem) on the uncertainties.

1. Charge Q and screening length λ

The average charge of microspheres Q and the screening length λ were needed as inputs in calculations of the interparticle force, which we then used to compute the shear stress $P_{xy}(t)$. The shear stress, in turn, was used in Eq. (S1) the time average entropy production rate in Eq. (S1).

We determined Q and λ using the method of Ref. [40]. In this method, experimentally obtained phonon spectra for our dusty plasma in a crystalline state were fit to a theoretical dispersion relation for particles with a Debye-Hückel interactions in a Wigner crystal. We obtained values for the two free parameters in the fit, $\kappa = 0.882$ and $\omega_{pd} = 74\ s^{-1}$. From these free parameters, we compute the average charge Q from $\omega_{pd} = \left(Q^2/2\pi\epsilon_0 m a^3\right)^{1/2}$ and the screening length λ from $\kappa = a/\lambda$.

The error bars in the values of Q and λ, while they do not affect our conclusions, merit some explaining regarding how we obtain them. To obtain the error bars, we use contours of χ^2 for the shielding parameter κ and dust plasma frequency ω_{pd}. While we did not find contours of χ^2 for our experiment, contours were obtained in another dusty plasma experiment under similar conditions, Ref. [41]. Using their contours, we estimated the uncertainties for Q and λ in our experiment. These estimated uncertainties were 7.6% for Q and 23% for λ, and these uncertainties were correlated in such a way that their contributions to the interparticle potential, Eq. (S5), largely cancelled out. To show that our results are insensitive to these uncertainties, systematic errors equivalent to the estimated uncertainty were added to Q and λ. Repeating the analysis with these additional errors, we found that the time averaged entropy production rate still obeyed the ECM fluctuation theorem.

Besides the steady-state values of charge and its error bars, there are other small effects on the charge of microspheres which have no bearing on our results, as we explain here. These effects are stochastic fluctuations, flow velocity effects, and depletions of electrons (Havnes effect).

Stochastic fluctuations of charge occur, but at too fast a time scale to matter. These fluctuations occur because individual electrons and ions are collected on the microsphere's surface at random times from the ambient plasma. The time scale for these charge fluctuations to occur is a multiple of the charging time, which is $\tau = K_t\,(kT_e)^{1/2}\,(an)^{-1}$, where T_e is the electron temperature, a is the radius of the microsphere, n is the plasma density, and K_τ is a function of the temperatures and masses of the ions and electrons[42,43]. For our plasma parameters, the charge fluctuations in our experiment occurred on a time scale of microseconds. On the other hand, the time scale for the motion of microspheres to respond to forces is characterized by the inverse dust plasma frequency, ω_{pd}^{-1}, which is the typical time

scale for the motion of a microsphere to be significantly deflected. For the microspheres in our dusty plasma, ω_{pd}^{-1} = 14 ms. Comparing these two time scales, we see they differ by four orders of magnitude. While the charge fluctuates, it does so much too fast to affect the motion of microspheres. Moreover, the magnitude of these charge fluctuations was small; we estimate that the charge fluctuations in our experiment were less than 1% of the time average charge, based on Eq. (13) of Ref. [42], which is consistent with counting statistics[42,44].

Variation of the charge due to whether a microsphere is in the fastest vs. the slowest part of the shear flow is also of no consequence. In the lab frame, the microspheres flow with velocities on the order of 1 mm/s, which was six orders of magnitude slower than the ion flow speed of 1 km/s. Using the standard model of Whipple[19], we find that a microsphere moving at the flow velocity of 1 mm/s has, at most, a one part in 10^6 difference in charge as compared to a stationary microsphere. This miniscule difference has no effect on our assumption that the charge of microspheres remains essentially constant.

Depletion of electrons also has a negligible effect on the charge of microspheres in our experiment. The so-called Havnes effect[45], which is applicable when particles of a substantial number density fill a three-dimensional volume, can reduce the charge of particles. This effect is miniscule in an experiment such as ours because our microspheres were levitated in a razor thin and sparse 2D layer within the plasma. Electrons and ions filled a large three-dimensional volume. Due to the ambient electric fields in the plasma, a fresh supply of electrons and ions from this three-dimensional volume constantly flowed past the small number of microspheres in their monolayer, so that the charge of the microsphere was determined by electrons and ions originating from outside the layer of microspheres.

2. Mass m of microspheres

The mass m of microspheres enters both the denominator and numerator of Eq. (S1) in the kinetic temperature T and the shear stress $P_{xy}(t)$, Eq. (S3), respectively.

We obtained the mass of the microspheres using the manufacturer's specifications of diameter (8.69 μm) and mass density (1.510 kg/m^3). Typical uncertainties of the mass are about 10%, which arise from the tendency for the masses of microspheres to change during storage and the experiment. This occurs primarily for two reasons. First, outgassing of volatile components can cause microspheres to shrink[41,46,47]. Second, sputtering in the plasma can cause the microsphere to either increase or decrease in size. The microspheres increase in size when the electrode is sputtered and deposited on the microspheres in high-power plasmas[47], while the microspheres decrease in size when the microspheres themselves are sputtered in low-power plasmas[48].

Uncertainty in the mass of the microspheres does not directly affect our results. When computing σ_τ using Eq. (S2), the mass m enters both the numerator and the denominator so that the mass term cancel. The entropy production rate has no direct dependence on mass, but rather depends on the dust plasma frequency ω_{pd}, which we measure directly from our experiment using the phonon spectra fitting method[40] described in section C1.

3. Microsphere positions and velocities

The positions and velocities of individual microspheres were used in computing the shear stress, Eq. (S3), as well as computing the shear rate γ and kinetic temperature *T*.

When obtaining time series of individual microspheres positions and velocities, there are random errors in position associated with measuring microsphere positions from raw video images[30] and consequently, random errors in velocity[31]. Typical errors in microsphere positions are about 0.05 pixels = 0.002*a*, where *a* is the Wigner-Seitz radius. Typical velocity errors are approximately 0.05 mm/s.

As a verification test to ensure that our results are insensitive to these errors, we began by adding additional artificial errors to the positions and velocities of individual microspheres. Then we repeated the analysis for the ECM fluctuation theorem using these new positions and velocities. The artificial errors in this verification test were chosen randomly from a Gaussian distribution centered at 0 with a standard deviation larger than the typical measurement errors. Even with these artificial errors, our result that our strongly coupled plasma obeyed the ECM fluctuation theorem did not change.

4. Shear rate γ

The shear rate γ was used to compute the time average entropy production rate σ_τ in Eq. (S1).

The shear rate γ used in Eq. (S1) can be computed two ways, and in either case, our strongly coupled plasma data satisfied the ECM fluctuation theorem. In the Letter, γ was computed as the transverse gradient of the flow velocity profile. The flow velocity profile was obtained from a spatial and time average of microsphere velocities[49]. In this case, γ was a single, constant value. Alternatively, a local and fluctuating shear rate $\gamma_t(t)$ within the rectangle that defines our subsystem could be computed. This fluctuating shear rate was computed from the *N = 56* microspheres within our subsystem and then time averaged over the time interval τ.

The uncertainty in γ was small when γ was obtained using the method presented in the Letter, where γ was computed as the transverse gradient in the flow velocity profile. The uncertainty in γ was 3.5%, which is small compared to uncertainties that arise from counting statistics when computing the LHS of Eq. (1).

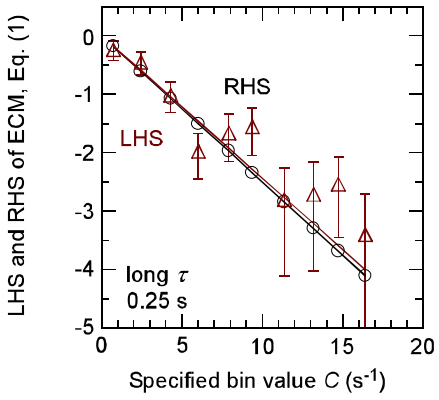

Supplementary Figure S2. **The ECM fluctuation theorem satisfied using a fluctuating shear rate.** The LHS and RHS of Eq. (1) agree for τ = 0.25 s. The LHS and RHS were obtained as in the Letter, except a fluctuating shear rate $\gamma_t(t)$ rather than the constant shear rate γ was used to compute entropy production rates.

When we used a fluctuating local shear rate $\gamma_t(t)$ to compute σ_τ, Eq. (S2), the resulting distribution of σ_τ still satisfied the ECM fluctuation theorem as shown in Supplementary Figure S2. However, the

distributions of the σ_τ changed substantially, so it is not clear whether the agreement with ECM for a fluctuating shear rate would hold for other experiments.

D. Another indication of our experimental data satisfying the ECM fluctuation theorem

Another indication that our strongly coupled plasma obeys a steady-state fluctuation theorem is that not only do the LHS and RHS agree for a long τ, they also both fall on a straight line in Fig. 3a,b. This linearity for the LHS data points was described by Gallavotti and Cohen[28] as their "key test of the theory." Our data satisfy this key test not only for the two values of τ, in Fig. 3a,b, but for all values that we tested.

E. Verification of our chief result for other numbers of microspheres *N* in the subsystem

To verify that our chief result (our strongly coupled plasma obeys the ECM fluctuation theorem) is not peculiar to our choice of *N*, we repeated the analysis of our experiment over the widest range of *N* practical for us. We found that our chief result was unaffected by the choice of *N*.

1. Our chief result is unchanged for N up to 75 microspheres

As an example of our tests for varying the size *N* of the subsystem, below are results for $N = 75$, showing that our conclusions remain the same for this size of subsystem.

Repeating the analysis of Eq. (1) for a slightly larger subsystem of $N = 75$ microspheres reveals a similar convergence of the LHS and RHS as we found for $N = 56$ microspheres. The discrepancies *D* between the LHS and RHS of Eq. (1) are presented in Supplementary Figure S2. There was a slightly shorter convergence time of $t_c = 0.031$ s for a subsystem of $N = 75$ microspheres as compared to $t_c = 0.037$ s for a subsystem of $N = 56$ microspheres.

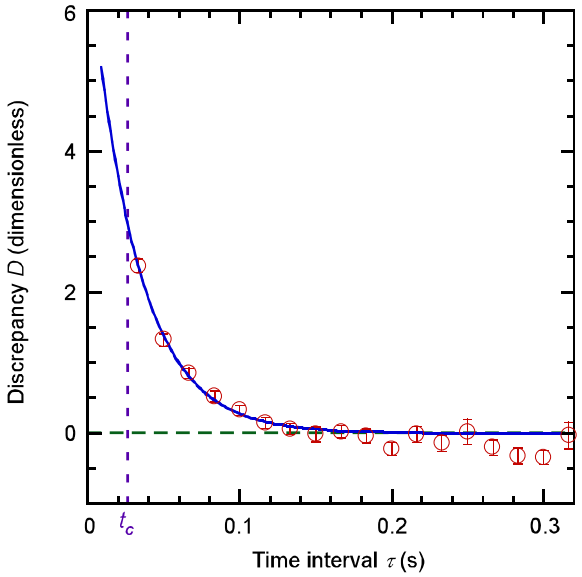

Supplementary Figure S3. **Convergence of the ECM fluctuation theorem for $N = 75$ microspheres.** This plot is analogous to Fig. 4 in the Letter. Using a larger subsystem of $N = 75$ microspheres, our dusty plasma still obeys the ECM fluctuation theorem. The LHS and RHS of Eq. (1) converge together as τ increases, just as it did for 56 microspheres. Discrepancies *D* and its errors were found just as in the Letter. Here, we find a convergence time $t_c = 0.031$ s for $N = 75$ microspheres as compared to $t_c = 0.037$ s for $N = 56$ microspheres.

The reason we did not explore subsystem sizes larger than N = 75 microspheres is the need for adequate statistics. There are two reasons that choosing a larger value of N would result in inadequate statistics for our experiment:

- The limited spatial size of the camera's field of view. The number of microspheres in the shear flow imaged by the camera was limited, which provides an absolute maximum for the N that we can study. Additionally, as N is increased substantially, the shear flow cannot be divided into as many subsystem of N microspheres.

- Rarity of negative fluctuations in entropy production rate for larger subsystems. As the number of microspheres in the subsystem was increased, the probability of negative entropy production events decreased. Having fewer negative entropy production events made it difficult to have sufficient statistics to compute the LHS of Eq. (1).

2. Role *of the shape of subsystem for very small subsystems*

We found that for very small subsystem of size N = 10, the entropy production rates generally obeyed the ECM fluctuation theorem. Interestingly, however, if we chose subsystems with an extreme aspect ratio (ratio of length to width), the LHS and RHS of Eq. (1) did not necessarily converge. For a subsystem with an aspect ratio of 0.52, the LHS and RHS converged together for long τ as the discrepancy D diminishes, as shown in Supplementary Figure S4a. For a subsystem with an extreme aspect ratio of 18.75, the LHS and RHS did not converge for long τ, as shown in Supplementary Figure S4b.

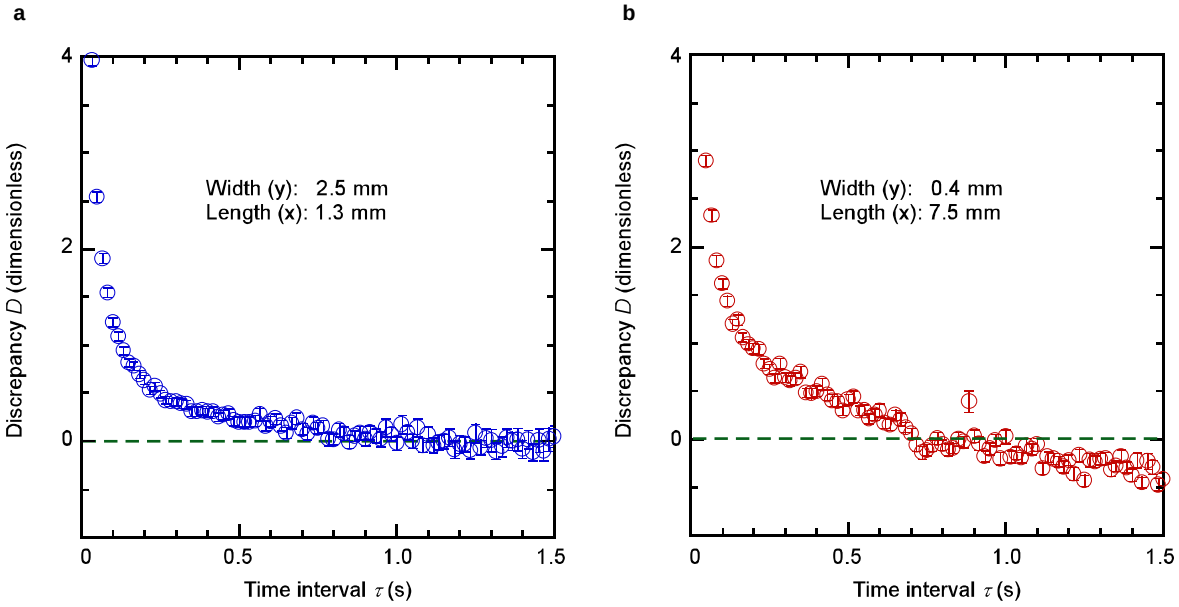

Supplementary Figure S4. **Subsystem shape dependence for ECM fluctuation theorem for *N* = 10 microspheres. a,** Convergence of the LHS and the RHS of Eq. (1) can be seen at long time intervals τ as the discrepancy *D* approaches 0. In this case, the subsystem's width (in the y-direction) was 2.5 mm, equivalent to the width of the subsystem used for *N* =56 microspheres. The average length (in the x-direction) was 1.3 mm. **b,** For an extreme case of a much longer box (width of 0.4 mm and length of 7.5 mm), the two sides of Eq. (1) did not converge together at long τ.

F. Description of how Ω_E was calculated

In the Letter, we reported our measurement of a convergence time t_C, which can provide insight into our physical system. To put this convergence time into context of other physical time scales of our dusty plasma, we compared the convergence time to the inverse entropy production rate, as well as the Einstein frequency Ω_E.

In a gas, a collision frequency expresses the inverse time scale for a particle's velocity to be scattered significantly by a binary collision. This idea of a collision frequency fails in a liquid because the collisions are not intermittent binary events, but constant deflections by multiple neighbors. Due to this failure, the terminology "collisional frequency" is seldom used in liquid physics. In the well-known textbook for liquids, *Theory of Simple Liquids* by Hansen and McDonald[50], the term "collision frequency" is only used twice in over 500 pages.

In a liquid, the concept of an Einstein frequency Ω_E is sometimes borrowed from the field of condensed matter physics to use as a proxy for a collision frequency. The Einstein frequency expresses the rate that a particle undergoes large deflections in its velocity due to the collective effects of multiple neighbors. Most often, the Einstein frequency is used to describe a crystal, but it has been used to describe a liquid dusty plasma[51] as we do.

The Einstein frequency is calculated using a theoretical abstraction that the motion of one particle *i* (that is free to move) among multiple neighbors *j* that are frozen in their positions. The motion of particle *i* is then described by a complicated potential well formed by the frozen neighbors.

The only data required to compute the Einstein frequency are the instantaneous positions of particles at just one moment in time. Also required is a formula for the forces between them, as a function of interparticle distance, and for this we use the binary Debye-Hückel potential, Eqs. (S4-S5). The key step in our procedure is to numerically calculate a distribution of values for derivative $k = df/dr$, and to use this distribution's mean to calculate $\Omega_E = \left\langle \sqrt{k/m} \right\rangle = 42 \text{ s}^{-1}$.

G. Molecular dynamics simulation to verify our chief result

As a verification that our chief result (a strongly coupled plasma obeys the ECM fluctuation theorem) was due to the shear flow and not due to the gas friction or anisotropy that were also present in the experiment, we performed a two-dimensional (2D) molecular dynamics (MD) simulation. Dusty plasmas are very well suited for comparison to MD simulations because the experiments generate particle-tracking data is analogous to the data generated by the simulations.

While the simulation mimicked the parameters of our experiment, the simulation was a simpler physical description because it excluded the following effects that were present in the experiment:

- The gas friction. In the experiment the microspheres experienced a gas friction force, proportional to their velocities. This gas friction dissipated heat. (The heat was generated viscously by Coulombic collisions among the microspheres that were undergoing shear motion.) The dissipation of heat, in balance with the laser heating, determined the kinetic temperature of the microspheres in the experiment. In the simulation, heat was also generated viscously, however, the temperature was held constant by a different mechanism: a Gaussian thermostat that constantly removed heat. This thermostat frequently rescaled peculiar velocities in the simulated area.

- The anisotropic temperature from using only two moving laser beams that gave kicks to microspheres in the $\pm$ *x* directions only. This anisotropy was previously described in Refs. [24,25].

Like the 2D simulation that was presented in the original fluctuation theorem paper of ECM[14], our simulation used the so-called SLLOD algorithm with Lees-Edwards boundary conditions. As mentioned above, viscous heat generated by the shear flow was extracted by a Gaussian thermostat that rescales the peculiar velocities of particles to keep the kinetic temperature constant. The equations of motion for the particles[52] were

$$\dot{\mathbf{q}}_i = \frac{\mathbf{p}_i}{m} + \gamma y_i \hat{\mathbf{x}} \tag{S6}$$

and

$$\dot{\mathbf{p}}_i = \mathbf{F}_i - \gamma p_{yi} \hat{\mathbf{x}} - \alpha \mathbf{p}_i \,, \tag{S7}$$

where $\boldsymbol{q}_i$ is position of particle *i*, $\mathbf{p}_i$ is a peculiar momenta of particle *i*, m is the mass of the particles, y_i is the vertical position of the particle *i*, γ is the shear rate, $\mathbf{F}_i$ is the net interparticle force acting on particle *i* due to all its neighbors, and α is the thermostat term. We integrated the equations of motion using a Verlet integrator.

Unlike the 2D simulation of ECM, we simulated a larger system of 1024 particles, from which we selected a subsystem of N = 56 particles. For this purpose, we used the rubber-banding method described in Section B as in the experiment, for a region with the same aspect ratio. Also unlike the ECM simulation, we used a Debye-Hückel interparticle potential to compute the force **F** in a way that mimics the experiment, instead of using a modified Lennard-Jones (Weeks-Chandler-Anderson) potential to mimic molecules. In computing **F**, we truncated the Debye-Hückel interparticle potential at distances greater than 11a, where a is the Wigner-Seitz radius.

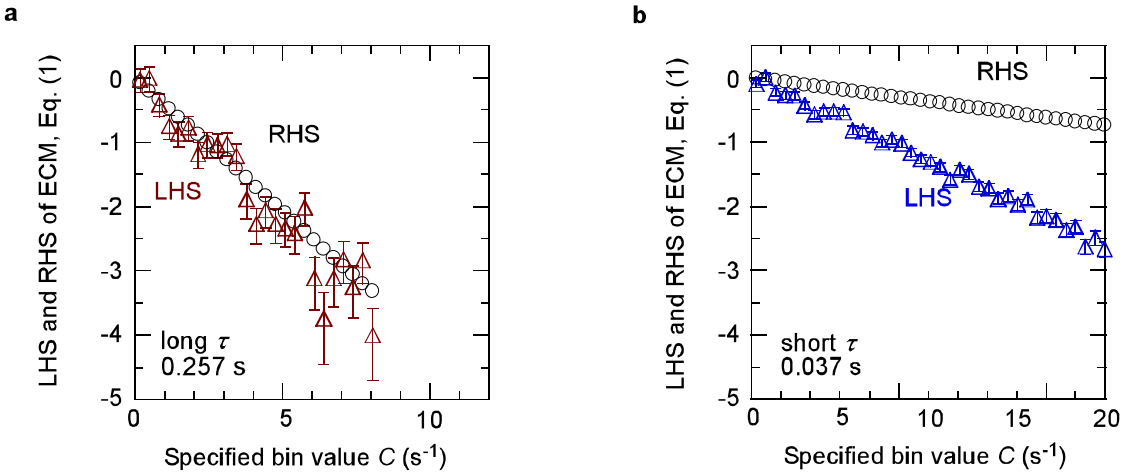

Supplementary Figure S5. **Demonstration of the fluctuation theorem using simulation data.** This figure is analogous to Fig. 3 in the Letter, but with an input of simulation data. **a,** A comparison of the LHS (triangles) and RHS (circles) of Eq. (1) computed from simulation data, for a long time interval, τ = 0.25 s. As the primary demonstration that our strongly coupled plasma obeys the ECM fluctuation theorem, we find that the LHS data points agree with the RHS data points within error bars for the simulation data, just as they did for experimental data. **b,** For a short τ, the LHS and RHS data points do not agree, consistent with the asymptotic aspect of Eq. (1), which was seen in the analysis of experimental data as well. The simulation data also satisfy Gallavotti and Cohen's "key test of the theory," as the LHS data points in **a,b** fall in a straight line. The LHS and RHS data points, as well as their error bars, for both **a,b,** were computed in the same way as in the Letter, but with an input of simulation data.

We chose simulation parameters to mimic the experiment. These included the same microsphere charge, microsphere mass, screening length, interparticle spacing, and shear rate as in the experiment. For the kinetic temperature, which was isotropic in the simulation, we chose a value midway between T_x and T_y of the experiment. The time step used in the simulation was 0.00021 s, which was chosen to provide energy conservation; this time step was much shorter than the 0.0167 s time between video frames in the experiment, so that the simulation produced a larger quantity of data.

The rest of the analysis for the ECM fluctuation theorem was done using our simulation data in the same manner as with experimental data in the Letter. The simulation results for the LHS and RHS of Eq. (1) for

a long τ and short τ are presented in Supplementary Figure S5. As in the experiment, we find that the LHS and RHS of Eq. (1) agree for a long τ (Supplementary Figure S5a), but not for a short τ (Supplementary Figure S5b). The convergence of the LHS and the RHS is demonstrated in Supplementary Figure S6, where the discrepancy D diminishes exponentially with τ. Here, for the simulation we find a convergence time of t_c = 0.052 s, which is similar to the experimental measurement of t_c = 0.037 s.

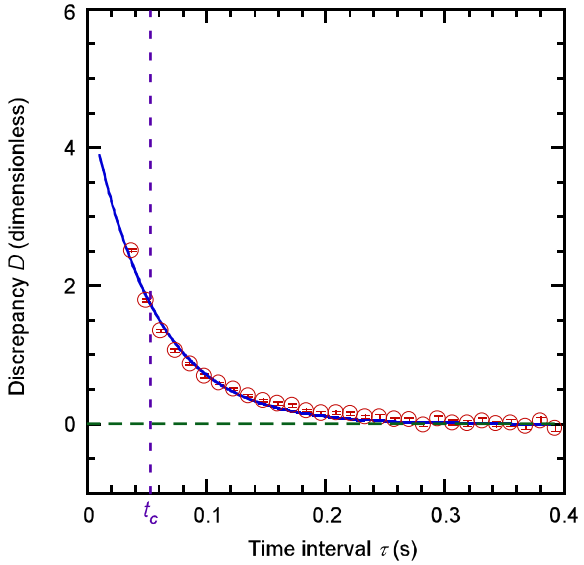

Supplementary Figure S6. **Convergence of the ECM fluctuation theorem for simulation data.** This plot for simulation data is analogous to Fig. 4 in the Letter for experimental data. Plotted are the discrepancies D between the LHS and RHS of Eq. (1). The LHS and RHS of Eq. (1) converge together as D diminishes for increasing τ, just as it did for experimental data. The discrepancies and their errors were computed in the same was as in the Letter. The convergence occurred exponentially, allowing us to obtain a convergence time t_c = 0.052 s for our simulation data as compared to t_c = 0.037 s for experimental data.

The similarity between our MD simulation results and experimental results shows that the salient element of the experiment responsible for agreement with the ECM fluctuation theorem was in fact the shear flow. The two effects that were excluded in our MD simulation (neutral gas friction and temperature anisotropy) did not play a major role in our chief result of demonstrating that our strongly coupled plasma obeys the ECM fluctuation theorem.

References:

31. Feng, Y., Goree, J. & Liu, B. Errors in particle tracking velocimetry with high-speed cameras. *Rev. Sci. Instrum.* **82**, 053707 (2011).

32. Hartmann, P., Kalman, G. J., Donkó, Z. & Kutasi, K. Equilibrium properties and phase diagram of two-dimensional Yukawa systems. *Phys. Rev. E* **72,** 026409 (2005).

33. Block, D. & Melzer, A. in *Introduction to Complex Plasmas* edited by Bonitz, M., Horing, N. & Ludwig. P, (Springer-Verlag, Berlin, Heidelberg, Germany, 2010), pp. 135-153.

34. Kalman, G., Hartmann, P., Donkó, Z. & Rosenberg, M. Two-Dimensional Yukawa Liquids: Correlation and Dynamics. *Phys. Rev. Lett.* **92,** 65001 (2004).

35. Avinash, K., Zhu, P., Nosenko, V. & Goree, J. Nonlinear compressional waves in a two-dimensional Yukawa lattice. *Phys. Rev. E* **68,** 46402 (2003).

36. Liu, B., Goree, J., Nosenko, V. & Boufendi, L. Radiation pressure and gas drag forces on a melamine-formaldehyde microsphere in a dusty plasma. *Phys. Plasmas* **10,** 9–20 (2003).

37. Otani, N. & Bhattacharjee, A. Debye Shielding and Particle Correlations in Strongly Coupled Dusty Plasmas. *Phys. Rev. Lett.* **78,** 1468–1471 (1997).

38. Konopka, U., Morfill, G. & Ratke, L. Measurement of the Interaction Potential of Microspheres in the Sheath of a rf Discharge. *Phys. Rev. Lett.* **84,** 891–894 (2000).

39. Lampe, M., Joyce, G., Ganguli, G. & Gavrishchaka, V. Interactions between dust grains in a dusty plasma. *Phys. Plasmas* **7,** 3851 (2000).

40. Nunomura, S. *et al.* Phonon spectrum in a plasma crystal. *Phys. Rev. Lett.* **89,** 35001 (2002).

41. Haralson, Z. & Goree, J. Temperature dependence of viscosity in a two-dimensional dusty plasma without the effects of shear thinning. *Phys. Plasmas* **23,** 093703 (2016).

42. Cui, C. & Goree, J. Fluctuations of the Charge on a Dust Grain in a Plasma. *IEEE Trans. Plasma Sci.* **22,** 151-158 (1994).

43. Choi, S. J. & Kushner, M. J. A Particle-in Cell Simulation of Dust Charging and Shielding in Low Pressure Glow Discharges. *IEEE Trans. Plasma Sci.* **22,** 138-150 (1994).

44. Piel, A. & Melzer, A. Dynamical processes in complex plasmas. *Plasma Phys. Control. Fusion* **44,** R1-R26 (2002).

45. Havnes, O., Aanesen, T. & Melandsø, F. On Dust Charges and Plasma Potentials in a Dusty Plasma With Dust Size Distribution. *J. Geophys. Res.* **95,** 6581–6585 (1990).

46. Pavlů, J. *et al.* Mass-Loss Rate for MF Resin Microspheres. *IEEE Trans. Plasma Sci.* **32,** 704-708 (2004).

47. Carstensen, J., Jung, H., Greiner, F. & Piel, A. Mass Changes of microparticles in a plasma observed by a phase-resolved resonance method. *Phys. Plasmas* **18,** 033701 (2011).

48. Mikikian, M. *et al.* Formation and behavior of dust particle clouds in a radio-frequency discharge: results in the laboratory and under microgravity conditions. *New J. Phys.* **5,** 19 (2003).

49. Feng, Y., Goree, J. & Liu, B. Energy Transport in a shear flow of particles in a two-dimensional dusty plasma. *Phys. Rev. E* **86,** 056403 (2012).

50. Hansen, J.-P. & McDonald, I. R. *Theory of Simple Liquids* 4^{th} *ed.* (Academic Press, Oxford, 2013).

51. Donkó, Z., Kalman, G. J. & Hartmann, P. Dynamical correlations and collective excitations of Yukawa Liquids. *J. Phys. Condens. Matter* **20,** 413101 (2008).

52. Evans, D. J. & Morriss, G. P. *Statistical Mechanics of Nonequilibrium Liquids* 2^{nd} *ed.* (ANU E Press, Canberra, 2007), p. 138.